Supporting Information

A platform efficiently produces aliphatic, aromatic, and heterocyclic primary diamines from alcohols

Zhizhen He[a], Yeting Han[a], Wei Song[a,b], Cong Gao[b], Xinmiao Liu[a], Wanqing Wei*[b] and Jing Wu*[a,b]

[a] School of Life Sciences and Health Engineering, Jiangnan University, Wuxi 214122, China;

[b] School of Biotechnology and Key Laboratory of Industrial Biotechnology of Ministry of Education, Jiangnan University, Wuxi 214122, China.

* Corresponding author: Jing Wu; Wanqing Wei

E-mail: wujing@jiangnan.edu.cn; wanqwei@163.com.

Content

Materials and Methods

General

Commercial reagents, standards, and solvents were purchased from Sigma-Aldrich (Shanghai, China), Meryer Chemicals (Shanghai, China), Aladdin Reagents (Shanghai, China), Macklin Reagent (Shanghai, China), and Bide Chemicals (Shanghai, China) used without further purification.

Strains and plasmids

E. coli DH5α and *E. coli* BL21 (DE3) were used as hosts for gene cloning and protein expression, respectively. The genes encoding the candidate alcohol dehydrogenases (ADHs) were chemically synthesized and ligated to plasmid pET-28a(+) by Talen-bio (Shanghai, China). The genes encoding glutamate dehydrogenase from *Saccharomyces cerevisiae* (*Sc*GluDH, UniProt ID: P07262) and single mutant (F91Y) of transaminase from *Escherichia coli* (*Ec*PaTA^{F91Y}, UniProt ID: P42588) were reserved by our Lab. Details of strains and plasmids used in this study were summarized in Table S5.

Construction of recombinant *E. coli* cells

DNA fragments of enzyme genes and the linear plasmid backbone were amplified by PCR using primers with 15 to 20 bp homologous arms that enabled the subsequent recombination. Full length of enzyme genes was assembled via overlap PCR and cloned into linear vector in the presence of 5 × CE II Buffer and Exnase II (Vazyme Biotech Co., Ltd., Nanjing, China) to generate 15 bp or

20 bp sticky ends to promote recombination efficiency. Reaction mixtures were 10 μL containing linear vector, enzyme genes, 5 × CE II Buffer and Exnase II, incubated in 37 °C for 30 min, followed by addition of 100 μL competent cells (*E. coli* DH5α) for transformation and plating on LB agar containing appropriate antibiotics. Resulting transformants were picked and DNA sequenced for confirmation. Plasmids containing targeted enzyme genes were transformed into *E. coli* BL21 cells for protein expression and whole-cell biocatalyst preparation. The detailed information of the strain and plasmids, primers and synthetic gene sequences were listed in Tables S5-S6.

Enzyme expression and preparation of whole-cell catalysts

Constructed *E. coli* cells were inoculated into 5 mL LB medium containing appropriate antibiotics (50 μg mL^{-1} kanamycin, 100 μg mL^{-1} ampicillin, 33 μg mL^{-1} chloramphenicol, 50 μg mL^{-1} streptomycin), and cultured at 37 °C, 220 rpm for 8 h. Precultures (3 mL) were transferred into 150 mL TB medium with appropriate antibiotics in 500 mL shaking flasks and cultured at 37 °C, 220 rpm for 2~3 h until the OD_{600} reached 0.8~1.0, then IPTG was added to give a final concentration of 0.4 mM. The temperature was shifted to 25 °C for 14h for protein expression (*Ec*ADH protein, the induction temperature was 16 °C for 18h). The cells were harvested by centrifugation at 8000 × g, 4 °C for 10 min, washed with 50 mM 4-(2-Hydroxyethyl) piperazine-1-ethanesulfonic acid buffer (HEPES, pH 8.0), then Centrifuge at 8000 × g for 10 minutes at 4 °C. Subsequently, collect the sedimented cells, which will either be used to obtain

purified enzymes or act as whole-cell biocatalysts in the following reactions.

Enzyme purification and kinetic assay

The cells were lysed using a high-pressure homogenizer. The resulting crude lysate was centrifuged at 10,000 × g at 4 °C for 30 min. The supernatant was collected, and the protein containing the His-tag was captured using a Ni-NTA Superflow resin for 30 min and then released using an elution buffer (20 mM Tris-HCl at pH 8.0, 0.3 M NaCl, and 0.5 M imidazole). Protein concentration was determined using a bicinchoninic acid protein assay kit (Solarbio, China), and purity was determined using sodium dodecyl-sulfate polyacrylamide gel electrophoresis.

The kinetic parameters of ADHs were monitored by following UV absorption at a wavelength of 340 nm using a microplate reader (Synergy HT, BioTek, VT, USA). The assay mixture, which contained 1~200 mM **1a** or **2a**, 0.1 mM Zn^{2+}, and 2 mM $NADP^+$ in 50 mM HEPES buffer (pH 9.0), was incubated at 40 °C for 20 min. Then, 2 μM ADHs were added, and the change in the absorbance at 340 nm was immediately recorded. The concentrations of NADPH were quantified by continuously recording the changing of the absorbance at 340 nm (ε = 6.22 mM^{-1} cm^{-1}). One unit of enzyme activity is the amount of enzyme required to convert 1 μM of $NADP^+$ into NADPH in 1 min.

***In vitro* reaction**

Mixture preparation: purified *Ec*ADH, *Sc*GluDH, and *Ec*PaTA^{F91Y} enzymes

were mixed at equimolar concentrations (20 μM) and incubated with 5 g/L of substrate 1a, 20 mM L-Glu, 50 mM HEPES, 100 mM ammonium formate, 0.5 mM PLP, 1 mM NADP+, and 0.5 mM Zn^{2+} at pH 9.0. A 5 mL reaction mixture was placed in a 20 mL brown, light-protected vial. The vial was shaken at 220 rpm and incubated at 37 °C for 6 h. After completion, 1 mL of the reaction solution was transferred to a 2 mL Eppendorf tube. The reaction was terminated by heating the sample in boiling water for 10 min, then centrifuged at 12,000 × g for 10 min, and the supernatant was collected for HPLC analysis. All experiments were performed in triplicate.

Converting 1a by whole-cell catalysts

Mixture preparation: constructed *E. coli* cells expressing enzymes of *Ec*ADH (wild type or mutant), *Sc*GluDH and *Ec*PaTA^{F91Y} (wild type or mutant) were reacted with 10~30 g/L **1a**, 20 mM L-Glu, 100 mM HEPES, 200~500 mM ammonium formate, 0.5 mM PLP, 2 mM $NADP^{+}$, and 0.5 mM Co^{2+} at pH 9.0, final cell density was 12 g CDW/L. A 5 mL reaction mixture was placed in a 20 mL light-protected vial. The vial was shaken at 220 rpm and incubated at 40 °C for 24 h. Then, samples were prepared for HPLC analysis to determine the titers of **2a** and **2c**. All experiments were performed in triplicate.

Converting a~p by whole-cell catalysts.

Mixture preparation: *E. coli* C03 expressing enzymes of *Ec*ADH^{M7}, *Sc*GluDH and *Ec*PaTA^{W4} was reacted with 50 mM **a~p**, 20 mM L-Glu, 100 mM

HEPES, 200 mM ammonium formate, 0.5 mM PLP, 1 mM $NADP^+$, and 0.5 mM Co^{2+} at pH 9.0, final cell density was 12 g CDW/L. A 5 mL reaction mixture was placed in a 20 mL light-protected vial. The vial was shaken at 220 rpm and incubated at 40 °C for 24 h. Then, samples were prepared for HPLC analysis to determine the titers of **3a~3p**. All experiments were performed in triplicate.

Mutagenesis experiments

The experiments about protein engineering were performed using the whole-plasmid PCR with KOD-Plus-Neo. The whole plasmid PCR system (50 μL) was composed of KOD DNA polymerase (1 μL), 10 × KOD PCR Buffer (5 μL), 2 mM dNTP mix (5 μL), 25 mM MgSO4 (3 μL), template (50−200 ng), corresponding primers (10 μM with 1 μL), and sterilized water. The PCR product was digested with the DpnI quick-cutting enzyme at 37 °C for 30−45 min. The PCR products were transformed into *E. coli* BL21 (DE3) cells for the following screening or DNA sequencing (GENEWIZ, China). The mutant libraries of *Ec*ADH were shown in Tables S5-S7. Mutant library of *Ec*PaTA was shown in Table S8. The screening of mutants was carried out through whole-cell transformation experiments with **1a** as the substrate. The titer of **2c** was detected by HPLC to determine the mutants. The relative activity of a mutant was calculated as the titer of **2c** of the mutant divided by the titer of **2c** of the template strain.

HPLC analysis

The samples were filtered through a 0.22 μm organic membrane, and then the titer of product amines were determined via HPLC using a Dionex UltiMate 3000 VWD detector (Thermo Fischer Scientific, Germany), an Agilent Zorbax SB-Aq column (4.6 × 150 mm; Agilent Technologies, USA), and an UV detector (Thermo Fischer Scientific, Germany) under the following conditions: detection wavelength: 264 nm, automatic precolumn derivatization with o-phthalaldehyde (OPA), sample injection volume of 8 μL, sample mixed with 4 μL of OPA, a flow rate of 1 mL/min, and phase A consisted of a 10 mM K_2HPO_4 buffer, with the pH adjusted to 7.3 using formic acid. Mobile phase B consisting of phase A, methanol, and acetonitrile at 1:3:5 (v/v/v). The ratios between the phase A and phase B are 0 min (60:40), 2 min (45:55), 15 min (10:90), 19 min (10:90), 22 min (60:40) and 25 min (60:40). The statistical analysis software is Chromeleon 7.2, and the graphing software is OriginPro 2022.

MS analysis

Amines were determined by MS. The analytical conditions of MS were as follows: ionic mode is ESI^+, capillary voltage: 3.5 kV, cone voltage: 30 V, source block temperature: 100 °C, desolvation temperature: 400 °C, desolvation gas flow: 700 lit/h, cone gas flow: 50 lit/h, collision energy: 6/20 V, mass range: 20–1000 m/z, detector voltage: 1800 V. We used WATERS MALDI SYNAPT Q-TOF MS to complete the detection. The statistical analysis and graphing software are MassLynx V4.1.

Initial structure preparation

The *Ec*ADH structure was obtained from the RCSB Protein Data Bank (PDB ID: 7BU3), and the ligands ASP, GOL, and PEG were removed, chain B was selected as the single-chain structure. Due to the fact that the first amino acid residue of the B-chain of 7BU3 is Met 3, the sequence numbers of all amino acid residues were decreased by 2 to be consistent with the residue sequence numbers of *Ec*ADH. The *Ec*ADH^{M7} structure was obtained from the prediction of alphafold2. The protonation states of charged residues were determined at constant pH 9.0 based on pKa calculations via the H++ (http://biophysics.cs.vt.edu/H++) tool and the consideration of the local hydrogen bonding network. Residues H40, H162, H180 and H257 were assigned as HID, and H61, H96, H163, H187, H321 was assigned as HIE. All lysine and arginine residues were protonated, glutamic acid and aspartic acid residues were deprotonated. Residues C39 and C150 are coordinated with the catalytic Zn, so they are assigned as CYM. Similarly, C94, C97, C100 and C107 are coordinated with the binding Zn and are also assigned as CYM.

The prepared protein was neutralized by adding counterions and solvated into a truncated octahedron TIP3P[1] water box with a 10 Å buffer distance on each side. After equilibrated with a series of minimizations interspersed by short MD simulations during which restrains on the protein backbone heavy atoms were gradually released (with force constant of 10, 2, 0.1 and 0 kcal/(mol·Å^2)), the system was gradually heated up to 313K in 50 ps in which harmonic

potentials were used to positionally restrain the protein backbone heavy atoms (with force constant of 10 kcal/(mol·Å^2)), and finally the standard unrestrained MD simulation with periodic boundary condition at 313K and 1 atm was carried out for up to 100 ns.

Molecular docking

In the equilibrium trajectories of *Ec*ADH and *Ec*ADH^{M7} models, 2000 snapshots were selected and divided into 10 groups using a hierarchical agglomerative (bottom-up) approach[2]. Then, the structure of **2a** was fully optimized at the B3LYP/6-31G(d) level using the Gaussian 16 package[3]. Molecular docking was conducted using the Lamarckian genetic algorithm local search method implemented in AutoDock 4.2 and AutoDockTools-1.5.6[4]. The docking procedure was performed with a rigid-receptor conformation. A total of 100 independent docking runs were performed. Finally, appropriate conformations were selected as the binding conformations for the *Ec*ADH-**2a** MD simulations.

Molecular dynamic simulations.

All MD simulations were performed using AMBER 18[5]. The partial charges of **2a** were fitted with HF/6-31G(d) calculations, and the restrained electrostatic potential[6] protocol was implemented by the Antechamber module in the Amber 18 package. The force field parameter for **2a** were adapted from that of the standard general amber force field 2.0 (gaff2)[7], whereas the standard

Amber14SB force field was applied to describe the protein. Each system was initially neutralized with counterions and solvated with explicit TIP3P[1] water in a truncated octahedron box with a 10 Å buffer distance on each side. Each system was then equilibrated with a series of minimizations interspersed by short MD simulations during which restraints on the protein backbone heavy atoms were gradually released [with force constants of 10, 2, 0.1, and 0 kcal/(mol·Å^2)] and heated slowly from 0 to 313 K for 50 ps during which we applied a 10 kcal/(mol·Å^2) restraint on the protein backbone heavy atoms. Finally, the standard unrestrained 100 ns MD simulations was performed at constant temperature and pressure. Pressure was maintained at 1 atm and coupled with isotropic position scaling. The temperature was controlled at 313 K via the Berendsen thermostat method. Long-range electrostatic interactions were treated with the particle mesh Ewald[8] method and 12 Å cutoff was applied to both particle mesh Ewald and van der Waals interactions. A time step of 2 fs was employed along with the SHAKE algorithm for hydrogen atoms, and a periodic boundary condition was used. Atomic positions were stored every 2 ps for further analysis. Each system was checked for stability (structure, energy, and temperature fluctuations) and convergence (root-mean-square deviations, RMSD of structures).

Supplementary Tables

Table S1. Comparison of the production performance of primary diamines by this study with those in relevant literatures.

Target product		Substrate	Catalytic approach	Titer (g/L)	Conversion (%)	Productivity (g/(L·h))	Reaction time (h)	Catalyst dosage (g_{CDW}/L)	Ref
Aliphatic primary diamines	1,3-Diaminopropane	1,3-Propanediol	Whole-cell	0.15	4	0.006	24	12	This study
		Glucose	Microbial fermentation	13	NA	0.19	69	NA	Lee et al. [9] (2015)
	1,4-Diaminobutane	1,4-Butanediol	Whole-cell	2.7	62	0.11	24	12	This study
		Glucose	Microbial fermentation	42	52[c]	1.3	34	NA	Lee et al. [10] (2017)
	1,5-Diaminopentane	1,5-Pentanediol	Whole-cell	3.6	71	0.15	24	12	This study
		Glucose	Microbial fermentation	104	53[c]	1.47	65	NA	Joo et al. [11] (2018)
	1,6-Diaminohexane	1,6-Hexanediol	Whole-cell	5.2	90	0.22	24	12	This study
		L-lysine	Microbial fermentation	0.21	65	0.006	36	NA	Wang et al. [12] (2024)
		Cyclohexanol	Whole-cell	0.49	42	NA	NA	69	Yun et al. [13] (2022)
		Cyclohexanol	Whole-cell	1.7	73	0.07	24	24	Li et al. [14] (2023)
	1,7-Diaminoheptane	1,7-Heptanediol	Whole-cell	5.5	84	0.23	24	12	This study
		Cycloheptanol	Whole-cell	0.46	35	NA	NA	69	Yun et al. [13] (2022)
		Cycloheptanol	Whole-cell	1.6	81	0.066	24	24	Li et al. [14] (2023)

Table S1 (Continued) Comparison of the production performance of primary diamines in this study with relevant literature.

Target product		Substrate	Catalytic approach	Titer (g/L)	Conversion (%)	Productivity (g/(L·h))	Reaction time (h)	Catalyst dosage (g_{CDW}/L)	Ref
Aliphatic primary diamines	1,8-Diaminooctane	1,8-Octanediol	Whole-cell	6.3	87	0.26	24	12	This study
		Cyclooctanol	Whole-cell	0.32	22	NA	NA	69	Yun et al. [13] (2022)
		Cyclooctanol	Whole-cell	1.7	79	0.071	24	24	Li et al. [14] (2023)
		n-Octane	Whole-cell	0.50	35	0.008	48	NA	Yun et al. [15] (2024)
	1,9-Diaminononane	1,9-Nonanediol	Whole-cell	6.2	78	0.26	24	12	This study
		1,9-Nonanediol	Whole-cell	1.3	81	0.21	6	10.8	Park et al. [16] (2024)
	1,4-Bis(aminomethyl)cyclohexane	1,4-Cyclohexanedimethanol	Whole-cell	23	77	0.95	24	12	This study
Aromatic primary diamines	*p*-Xylylenediamine	*p*-Phenylenedimethanol	Whole-Cell	4.3	63	0.18	24	12	This study
		Terephthalic acid	Purified enzyme	1.3	39	0.054	24	NA	Kunjapur et al. [17] (2023)
	m-Xylylenediamine	*m*-Phenylenedimethanol	Whole-Cell	3.5	51	0.147	24	12	This study
Heterocyclic primary diamines	2,5-Bis(aminomethyl)furan	2,5-Furandimethanol	Whole-Cell	1.1	17	0.044	24	12	This study
		5-Hydroxymethylfurfural	Purified enzyme	10.7	85	0.36	30	NA	Yun et al. [18] (2024)

c：Calculated based on the yield g/g glucose. NA means no available data.

Table S2. Substrate and product pricesa

Brand	Country	1,6-Hexanediol (£/kg)	1,4-Dicyanobutane (£/kg)	L-lysine (£/kg)	Cyclohexanol (£/kg)	1,6-Diaminohexane (£/kg)	*p*-Phenylenedimethanol (£/kg)	Terephthalonitrile (£/kg)	Terephthalic acid (£/kg)	*p*-Xylylenediamine (£/kg)	2,5-Furandimethanol (£/kg)	5-hydroxymethylfurfural (£/kg)	2,5-Bis(aminomethyl)furan (£/kg)
Thermo Fisher Scientific	United States	45.9	68.3	NA	35.4	102.8	NA	NA	44.1	NA	NA	NA	NA
Accel Scientific	Spain	10.1	NA	27	9.3	NA	57.1	35.3	5.4	NA	919	NA	NA
Aurum Pharmatech	United States	16.9	64	61.7	40.9	115	74.2	65.7	9.6	829	1227	NA	7319
Adamas	China	6.74	19.2	26.7	6.6	17.1	59.9	22.5	6.0	1872	924	104	9150
Energy Chemical	China	NA	13	24.2	6.5	20.8	NA	21.8	5.2	828	993	151	8603
Meryer	China	13.9	23.5	NA	5	41.2	77.8	22.9	6.7	1846	1006	414	NA
Aladdin	China	19.3	22.3	29.2	4.2	18.4	78.8	29.8	6.7	2184	1085	162	NA
Macklin	China	13.9	23.8	30.6	5.4	41.1	67.0	22.9	6.7	1070	982	171	12480
Average price		18.1	33.4	33.2	14.2	50.9	69.1	31.6	11.3	1438	1019	200	9388

a: The price was obtained from Scifinder and ChemSpider. NA means no available data.

Table S3. Comparison of cost-effectiveness of our method with reported processes.

Target product and its price.	Substrate	substrate cost* £/(kg product)	Reaction conditions (temperature, pressure).	Solvent	Titer g/L	Conversion %	Ref
Aliphatic primary diamines：	1,6-Hexanediol	18.4	40 °C 0.1 Mpa	Water	5.5	90	This study
1,6-Diaminohexane 50.9 £/kg	1,4-Dicyanobutane	31.1	100 °C 5 Mpa	Ethanol	NA	85	Liang et al [19] (2024)
	L-lysine	41.8	37 °C 0.1 Mpa	Water	0.21	65	Wang et al. [12] (2024)
	Cyclohexanol	12.2	25 °C 0.1 Mpa	Water	1.68	73	Li et al. [6] (2023)
Aromatic primary diamines：	*p*-Phenylenedimethanol	70.2	40 °C 0.1 Mpa	Water	4.3	63	This study
p-Xylylenediamine 1438 £/kg	Terephthalonitrile	29.7	70 °C 5 Mpa	Toluene	NA	97~99	Patent [20]
	Terephthalic acid	13.8	30 °C 0.1 Mpa	Water with 5% (v/v) DMSO	1.3	39	Kunjapur et al. [17] (2023)
Heterocyclic primary diamines:	2,5-Furandimethanol	1035.6	40 °C 0.1 Mpa	water	1.05	17	This study
2,5-Bis(aminomethyl)furan 9388 £/kg	5-hydroxymethylfurfural	200.4	20~37 °C 0.1 Mpa	Water with 10% (v/v) DMSO	10.7	85	Yun et al. [18] (2024)

*: Calculate the substrate cost per kilogram of product based on 100% conversion yield. NA means no available data.

Table S4. Candidate ADHs.

Enzyme	Sources	Uniprot ID	1a			2a		
			K_m [mM]	k_{cat} [min^{-1}]	k_{cat}/K_m [$min^{-1}\cdot mM^{-1}$]	K_m [mM]	k_{cat} [min^{-1}]	k_{cat}/K_m [$min^{-1}\cdot mM^{-1}$]
*Ec*ADH	*Escherichia coli.*	P27250(*)	7.3±0.5	262.0±4.2	36.2	14.3±2.6	42.2±0.1	3.0
*Syn*ADH	*Synechocystis sp.* PCC 6803	P74721	7.3±2.2	89.4±7.8	12.6	11.2±2.7	8.1±0.1	0.7
*Gt*ADH	*Geobacillus thermodenitrificans*	A4ISB9	6.3±0.4	60.6±4.8	9.6	7.4±0.3	18.6±0.1	2.9
*Pp*ADH	*Pelophylax perezi.*	O57380	6.6±0.7	44.2±1.2	6.6	3.9±0.8	3.3±0.1	0.8
*Aci*ADH	*Acinetobacter sp.* NCIMB9871	Q9F7D8	19.3±4.7	6.8±0.4	0.4		n.d.	
*Aa*ADH	*Aedes aegypti.*	D2WKD9		n.d.			n.d.	
*He*ADH	*Halomonas elongata.*	E1V3M3		n.d.			n.d.	
*Ac*ADH	*Acinetobacter calcoaceticus*	Q59096		n.d.			n.d.	

P27250(*): The amino acid sequence of *Ec*ADH is obtained by truncating the Met1 and Ser2 residues at the N-terminus of the sequence based on P27250. Data represent the mean ± SD from three replicates. n.d. means not detected.

Table S5. Plasmids and strains.

Plasmid	Description	Source
pET-28a(+)	single T7 promoters, pBR322 ori, Kan^R	Novagen
pRSFDuet-1	Double T7 promoters, RSF ori, Kan^R	Novagen
pETDuet-1	Double T7 promoters, pBR322 ori, Amp^R	Novagen
pCDFDuet-1	Double T7 promoters, CDF13 ori, Str^R	Novagen
pACYCDuet-1	Double T7 promoters, p15A ori, Cm^R	Novagen

Strain	Description	source
E. coli BL21 (DE3)	*F–ompT gal dcm lon hsdSB (rB– mB–) λ(DE3 [lacI lacUV5-T7 gene 1 ind1 sam7 nin5])*	Invitrogen
E. coli A01	pACYCDuet-1 carrying *Sc*GluDH and *Ec*ADH	This study
E. coli A02	pACYCDuet-1 carrying *Sc*GluDH and *Ec*ADHM7	This study
E. coli B01	pET-28a(+) carrying *Ec*PaTAF91Y	This study
E. coli B02	pET-28a(+) carrying *Ec*PaTAW4	This study
E. coli C01	pACYCDuet-1 carrying *Sc*GluDH and *Ec*ADH^{M7}, pET-28a(+) carrying *Ec*$PaTA^{W4}$	This study
E. coli C02	pRSFDuet-1 carrying *Ec*$PaTA^{W4}$(MCS-1) and *Ec*ADH^{M7}(MCS-2), pACYCDuet-1 carrying *Sc*GluDH	This study
E. coli C03	pRSFDuet-1 carrying *Ec*$PaTA^{W4}$(MCS-2) and *Ec*ADH^{M7}(MCS-1), pACYCDuet-1 carrying *Sc*GluDH	This study
E. coli C04	pETDuet-1 carrying *Ec*$PaTA^{W4}$(MCS-1) and *Ec*ADH^{M7}(MCS-2), pACYCDuet-1 carrying *Sc*GluDH	This study
E. coli C05	pETDuet-1 carrying *Ec*$PaTA^{W4}$(MCS-2) and *Ec*ADH^{M7}(MCS-1), pACYCDuet-1 carrying *Sc*GluDH	This study
E. coli C06	pCDFDuet-1 carrying *Ec*$PaTA^{W4}$(MCS-1) and *Ec*ADH^{M7}(MCS-2), pACYCDuet-1 carrying *Sc*GluDH	This study
E. coli C07	pCDFDuet-1 carrying *Ec*$PaTA^{W4}$(MCS-2) and	This study

*Ec*ADH^{M7}(MCS-1), pACYCDuet-1 carrying *Sc*GluDH

260

Table S6. Primer sequences.

Name	Function	Sequence (5'→3')
MCS1-F	Inverse PCR to amplify the linearized vector pRSFDuet-1, pETDuet-1, pCDFDuet-1, and pACYCDuet-1 with the Multiple Cloning Site 1 (MCS1) removed.	GCATAATGCTTAAGTCG
MCS1-R		ATTCGGATCCTGGCTGTGG
MCS2-F	Inverse PCR to amplify the linearized vector pRSFDuet-1, pETDuet-1, pCDFDuet-1, and pACYCDuet-1 with the Multiple Cloning Site 2 (MCS2) removed.	CAGCTTAATTAACCTAGGC
MCS2-R		CTTATACTTAACTAATATAC
MCS1-GluDH-F	The *Sc*GluDH with homologous arms of MCS1 can be amplified.	ACAGCCAGGATCCGAATATGTCAGAGCCTGAG
MCS1-GluDH-R		CGACTTAAGCATTATGCTTAGAAAACATCACCTTGG
MCS1-ADH-F	The *Ec*ADH with homologous arms of MCS1 can be amplified.	ACAGCCAGGATCCGAATATGATTAAATCCTATGC
MCS1-ADH-R		CGACTTAAGCATTATGCTTAATAATCAGCTTTAAGAACG
MCS2-ADH-F	The *Ec*ADH with homologous arms of MCS2 can be amplified.	ATTAGTTAAGTATAAGAAGGAGATATAATGATTAAATCCTATGC
MCS2-ADH-R		TAGGTTAATTAAGCTGTTAATAATCAGCTTTAAGAACG
MCS1-TA-F	The *Ec*PaTA with homologous arms of MCS1 can be amplified.	ACAGCCAGGATCCGAATATGAACCGTCTGCCGTC
MCS1-TA-R		CGACTTAAGCATTATGCTTAAGCTTCTTCTACAG
MCS2-TA-F	The *Ec*PaTA with homologous arms of MCS2 can be amplified.	ATTAGTTAAGTATAAGAAGGAGATATAATGAACCGTCTGCC
MCS2-TA-R		TAGGTTAATTAAGCTGTTAAGCTTCTTCTACAG

Table S7. Mutant library of *Ec*ADH M1 variants.

Region	Mutant
Loop 1	E49S, E49T, E49R, E49K, E49H, E49D, E49N, E49Q, E49G, E49V, E49M,
	E49C
	W50F, W50C
	G51S, G51D, G51K
	F52D, F52E, F52N, F52Q, F52W, F52L, F52S, F52T, F52K, F52R, F52H
Loop 2	Q105E
	I106D, I106E, I106N, I106Q, I106K, I106H, I106A, I106L, I106S, I106T
	A112L, A112I, A112P, A112T, A112N, A112Q, A112D
	P114L, P114I, P114G, P114A
Loop N	S198T
	N238C, N238S, N238D
	T258L, T258S, T258E, T258Q, T258R
	A261L, A261H, A261D, A261Q, A261R
	V262P
	L263D, L263E
	T264I, T264E, T264V, T264D
	S267E, S267K, S267R
	S283D, S283N, S283T
	A284L, A284S, A284G
	T285I, T285V, T285H

Note: Beneficial mutants are highlighted in red.

Table S8. Mutant library of *Ec*ADH M6 variants.

Template	Region	Mutant
M5	Loop 1	S53T, S53C, S53M, S53P Q54F, Q54T, Q54S, Q54P, Q54K, Q54M, Q54G, Q54A, Q54C Y55F, Y55V, Y55L, Y55S, Y55T, Y55C, Y55H, Y55D, Y55M, Y55Q

Note: Beneficial mutants are highlighted in red.

Table S9. Mutant library of *Ec*ADH M7 variants.

Template	Region	Mutant
		G88V, G88A, G88C
M6	Loop 3	W89C, W89Y, W89T
		T90S, T90D, T90E, T90N, T90F, T90A, T90V, T90L, A91G, A91V, A91I

Note: Beneficial mutants are highlighted in red.

Table S10. Mutant library of *Ec*PaTA variants.

	Mutant
Round 1	W1/F84Y, W1/S149T, W1/S153A, W1/F180Y, W1/S184T, W1/N214D, W1/L351E, W1/F370L, W1/A384V, W1/A416L, W1/T424V, W1/L433I，W1/F84Y/S184T(W3)
Round 2	W3/Q119N, W3/N148Q, W3/T151S, W3/V154A, W3/V154L, W3/H181K, W3/H181R, W3/V273A, W3/V273L, W3/T275S, W3/A299V, W3/A299G, W3/L419V, W3/L419I(W4), W3/R426K

Note: Beneficial mutants are highlighted in red.

Supplementary Figures

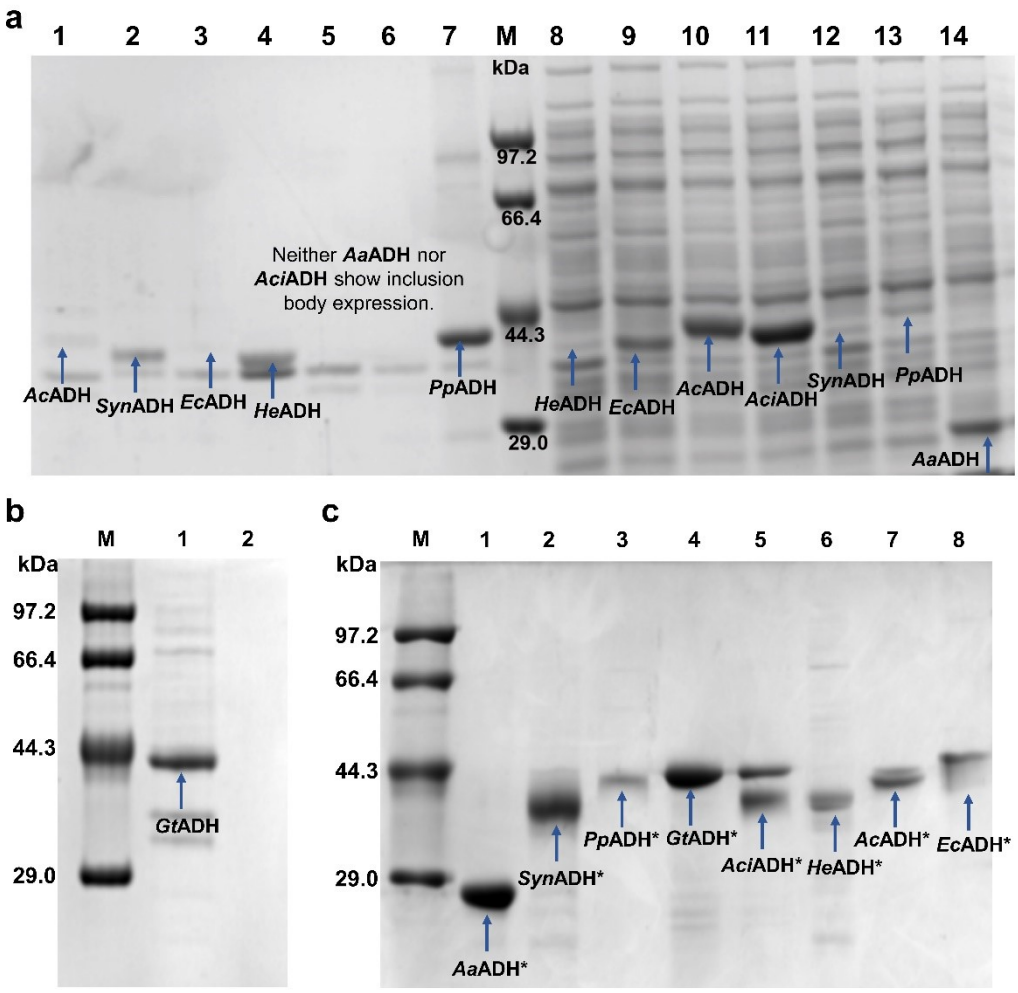

Figure S1. SDS-PAGE of eight candidate ADHs.

(a) The lanes for protein pellets are arranged as follows: *Ac*ADH, *Syn*ADH, *Ec*ADH, *He*ADH, *Aa*ADH, *Aci*ADH, *Pp*ADH. The lanes for protein supernatants are arranged as follows: *He*ADH, *Ec*ADH, *Ac*ADH, *Aci*ADH, *Syn*ADH, *Pp*ADH, *Aa*ADH. Lane M represents the protein marker; (b) Lane 1: *Gt*ADH supernatant; lane 2: *Gt*ADH pellet; (c) SDS-PAGE of the purified enzymes. Lane 1: *Aa*ADH, lane 2: *Syn*ADH, lane 3: *Pp*ADH, lane 4: *Gt*ADH, lane 5: *Aci*ADH, lane 6: *He*ADH, lane 7: *Ac*ADH, lane 8: *Ec*ADH. The asterisk (*) indicates enzymes carrying an N-terminal 6×His tag.

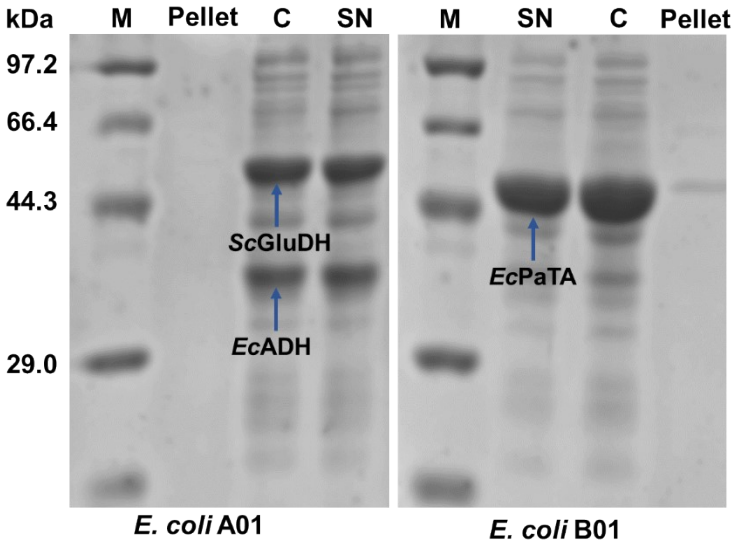

284

285 **Figure S2. SDS-PAGE of *E. coli* A01 and *E. coli* B01.**

286 Lane M represents protein marker, lane C represents whole cells, lane SN represents the

287 supernatant, and lane Pellet represents pellet.

288

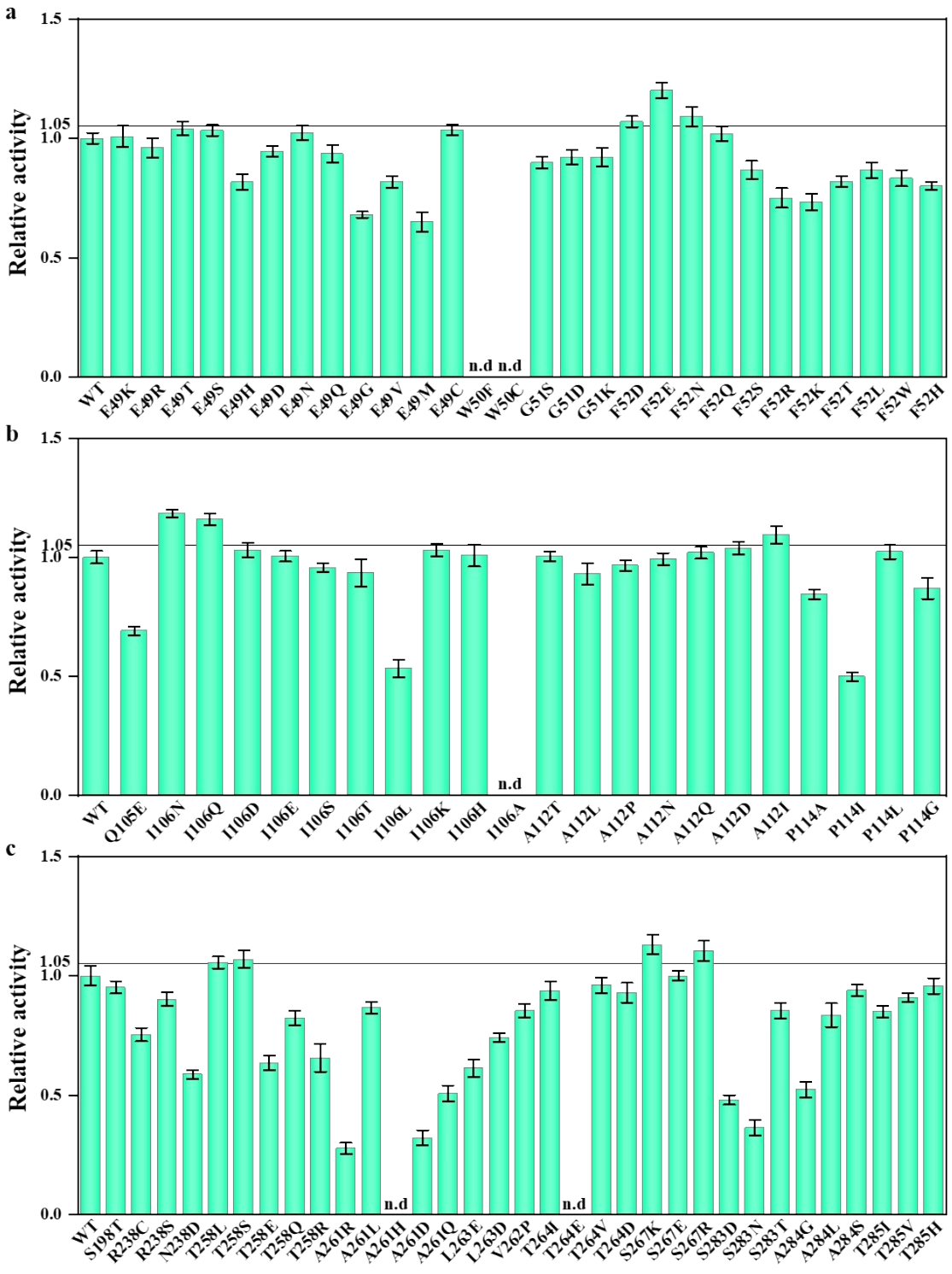

Figure S3. The single mutants of *Ec*ADH.

Conversion conditions: 10 g/L **1a**, 100 mM HEPES, 20 mM L-Glu, 200 mM ammonium formate, 0.5 mM PLP, 2 mM $NADP^+$, and 0.5 mM Co^{2+}. Reactions were carried out with 6 g/L CDW of *E. coli* A01 expressing ADH mutants and 6 g/L CDW of *E. coli* B01 at pH 9.0 and 40°C for 24 h. *n.d.* indicates **2c** product was not detected. Error bars indicate standard deviation of three independent replicates. Data represent the mean ± SD from three replicates.

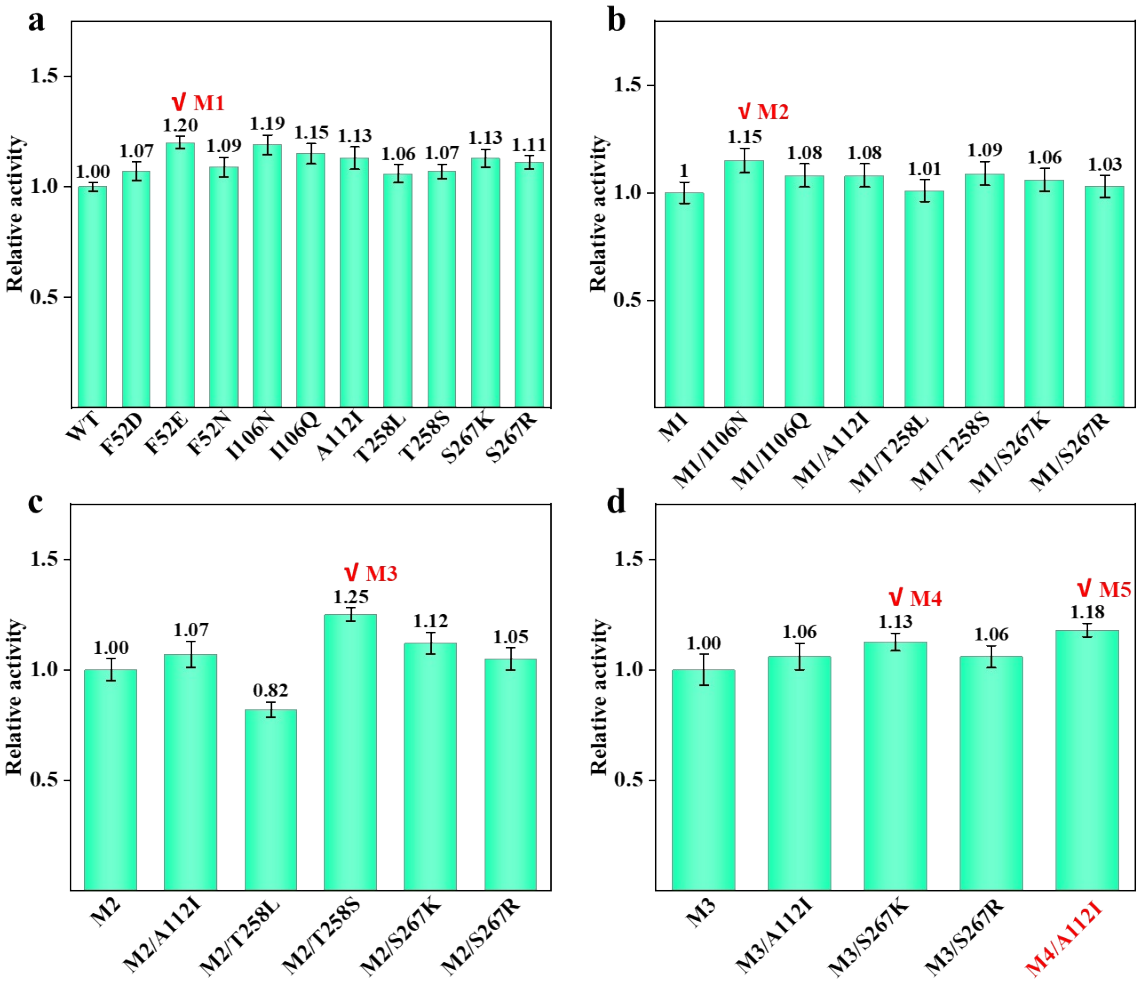

Figure S4. Mutants of *Ec*ADH(M1-M5).

(a) Beneficial single mutants with 10 g/L **1a** and 200 mM ammonium formate. (b) Beneficial double mutants with 10 g/L **1a** and 200 mM ammonium formate. (c) Beneficial triple mutants with 20 g/L **1a** and 400 mM ammonium formate. (d) Beneficial quadruple mutants with 30 g/L **1a** and 500 mM ammonium formate. Conversion conditions: 10-30 g/L **1a**, 50 mM HEPES, 20 mM L-Glu, 200–500 mM ammonium formate, 0.5 mM PLP, 2 mM $NADP^+$, and 0.5 mM Co^{2+}. Reactions were conducted with 6 g/L CDW of *E. coli* A01or *Ec*ADH mutants and 6 g/L CDW of *E. coli* B01 at pH 9.0 and 40°C for 24 h. Error bars indicate standard deviation of three independent replicates. Data represent the mean ± SD from three replicates.

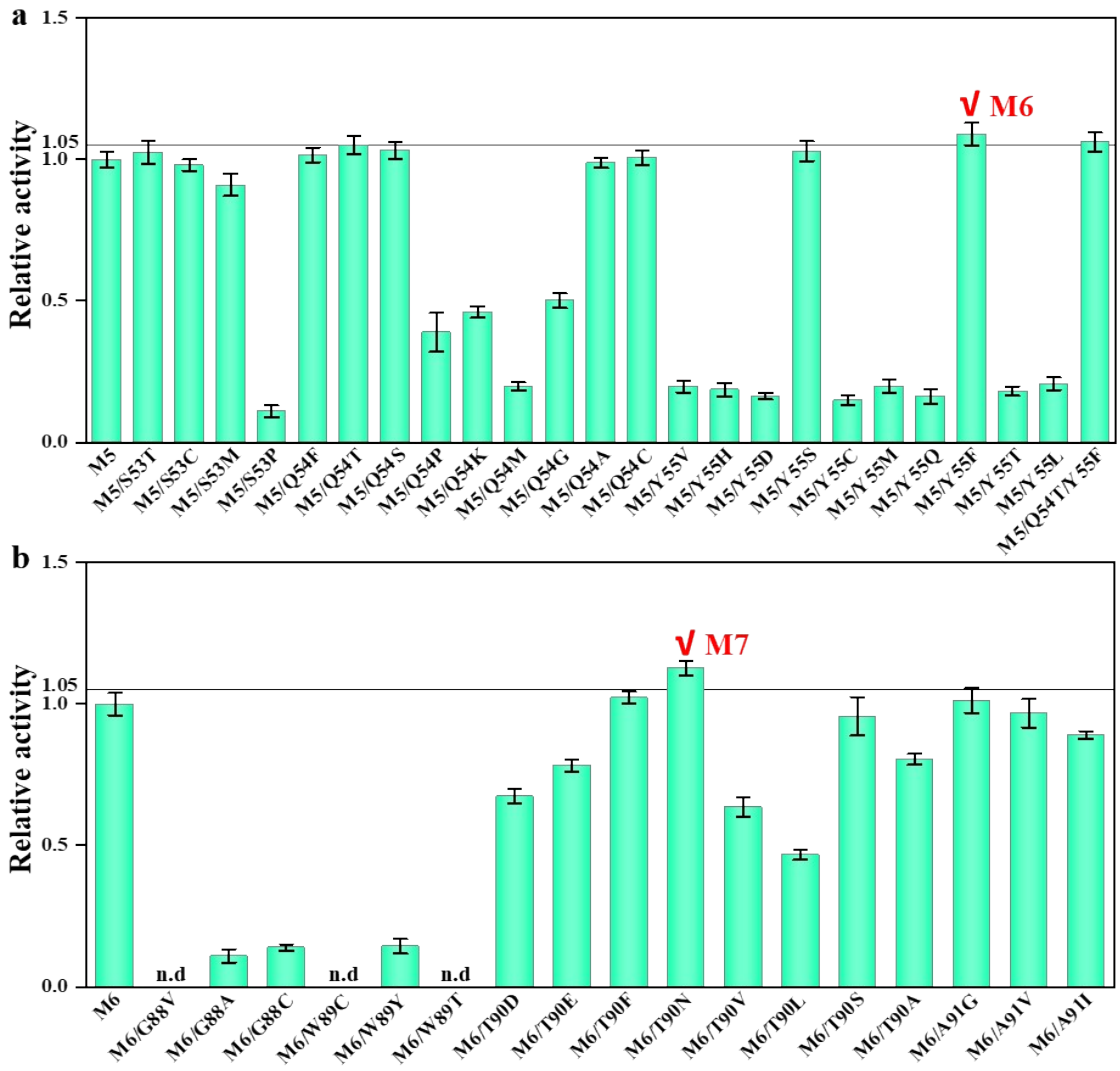

307

308 **Figure S5. Mutants of *Ec*ADH(M1-M7).**

309 (a) M6 mutants of *Ec*ADH. (b) M7 mutants of *Ec*ADH. Conversion conditions: 30 g/L **1a**, 50 mM
310 HEPES, 20 mM L-Glu, 500 mM ammonium formate, 0.5 mM PLP, 2 mM $NADP^+$, and 0.5 mM Co^{2+}.
311 Reactions were conducted with 6 g/L CDW of *E. coli* A01 or *Ec*ADH mutants and 6 g/L CDW of *E.*
312 *coli* B01 at pH 9.0 and 40°C for 24 h. n.d. indicates **2c** product was not detected. Error bars indicate
313 standard deviation of three independent replicates. Data represent the mean ± SD from three
314 replicates.

315

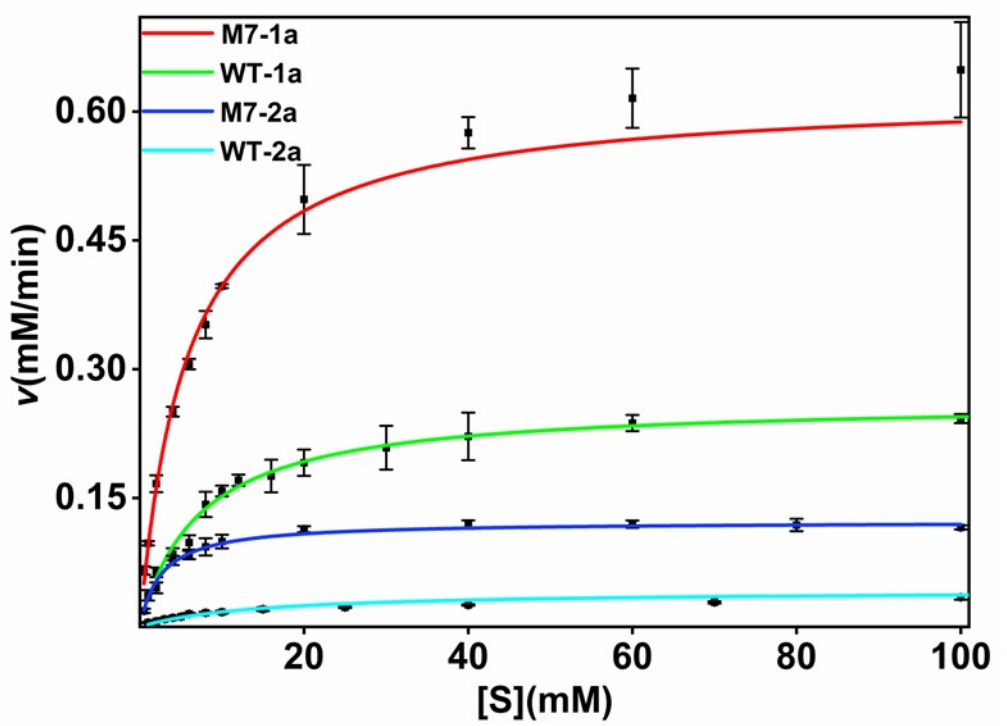

Model	MichaelisMenten			
Equation	y = Vmax * x / (Km + x)			
Plot	WT-1a	M7-1a	WT-2a	M7-2a
Vmax	0.26232 ± 0.00441	0.62118 ± 0.01777	0.04223 ± 0.00269	0.12242 ± 0.00173
Km	7.26147 ± 0.4694	5.65627 ± 0.38967	14.31014 ± 2.58217	2.60334 ± 0.21575
Reduced Chi-Sqr	0.97038	2.83727	14.5881	0.78751
R^2(COD)	0.98849	0.99747	0.93315	0.99351
Adj.-R^2	0.98753	0.99719	0.92837	0.99286

Figure S6. Kinetic parameters of *Ec*ADH wild-type (WT) and its mutant M7.

Error bars indicate standard deviation of three independent replicates. Data represent the mean ± SD from three replicates.

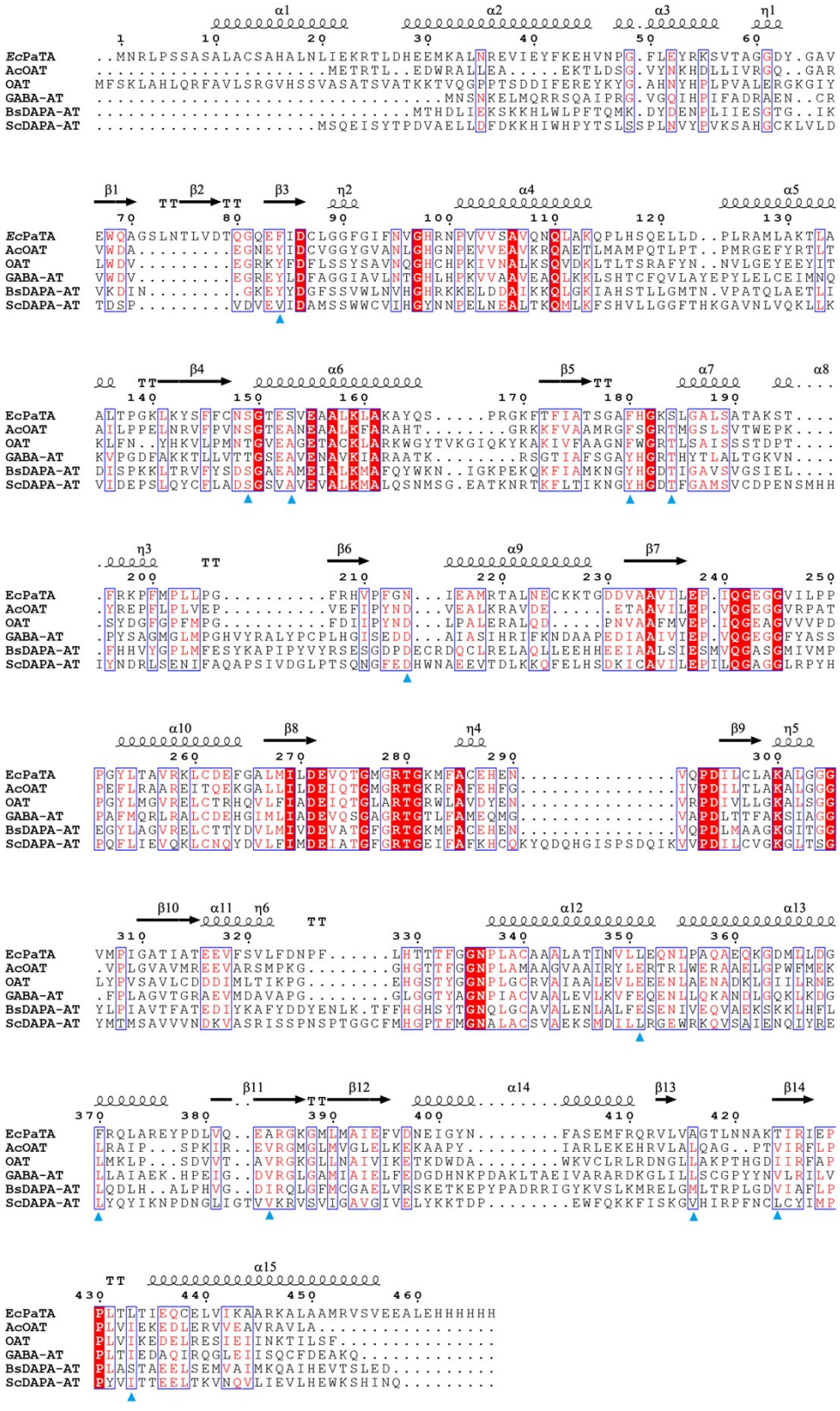

Figure S7. Sequence alignment of transaminases.[21]

*Ec*PaTA (PDB: 4UOX), AcOAT (PDB: 1VEF), OAT (PDB: 2OAT), GABA-AT (PDB: 1SFF), BsDAPA-AT (PDB: 1SFF), ScDAPA-AT (Uniprot: P50277).

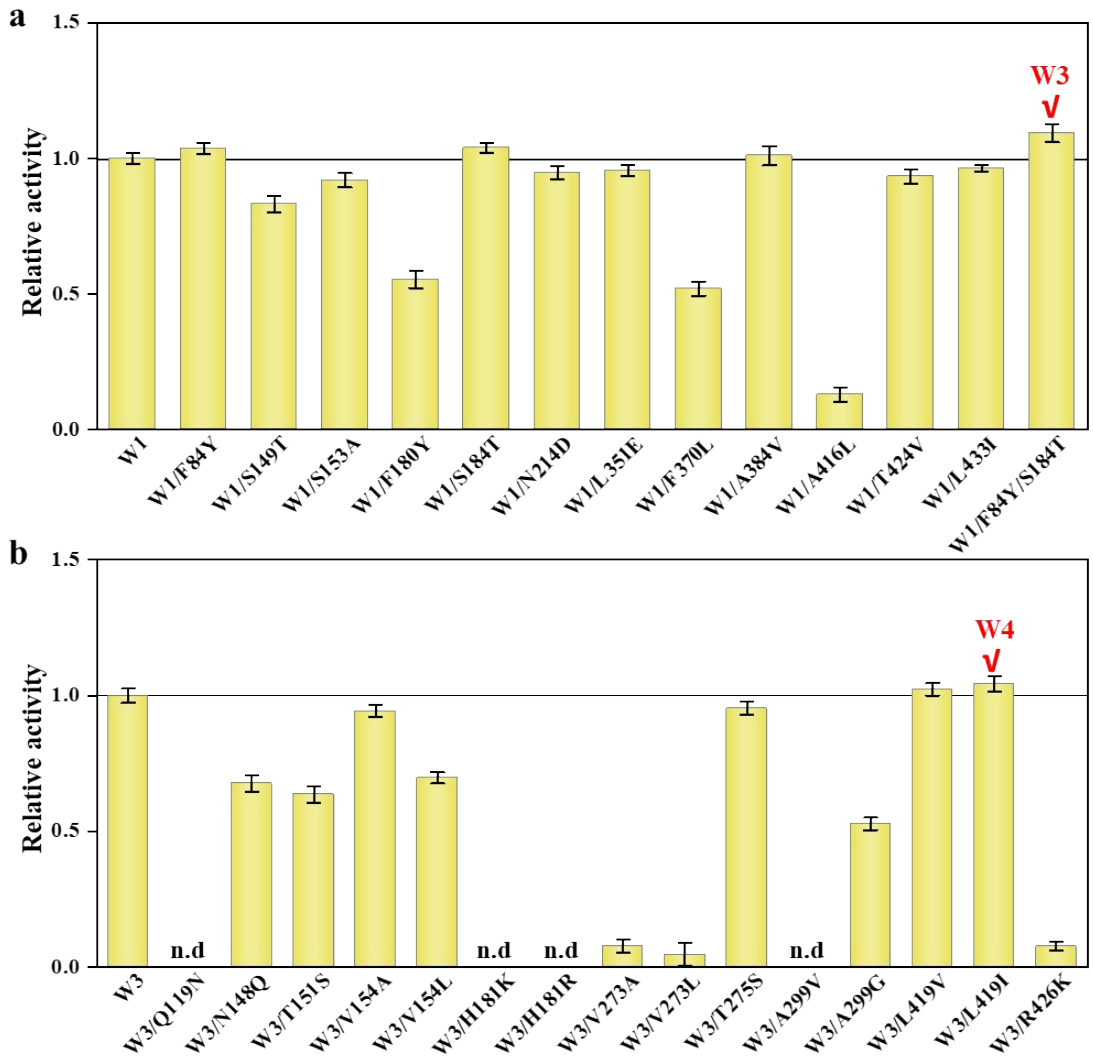

Figure S8. Mutants of *Ec*PaTA^{F91Y}.

(a) The first-round mutants. (b) The second-round mutants. Conversion conditions: 30 g/L **1a**, 50 mM HEPES, 20 mM L-Glu, 500 mM ammonium formate, 0.5 mM PLP, 2 mM $NADP^+$, and 0.5 mM Co^{2+}. Reactions were conducted with 6 g/L CDW of *E. coli* A02 and 30 g/L CDW of *E. coli* B01 or expressing transaminase mutants at pH 9.0 and 40°C for 24 h. n.d. indicates **2c** product was not detected. Error bars indicate standard deviation of three independent replicates. Data represent the mean ± SD from three replicates.

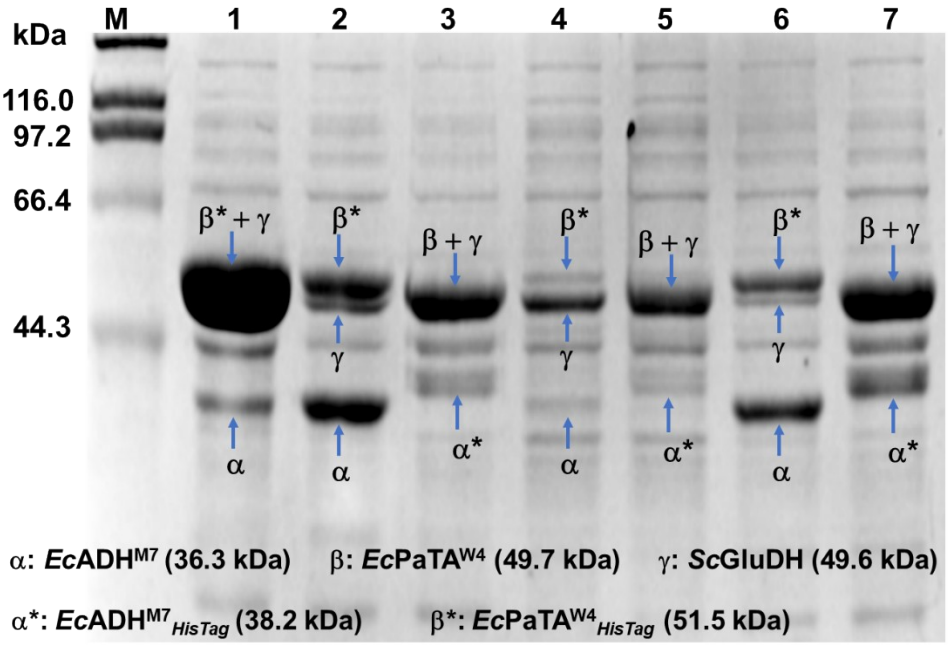

334

335 **Figure S9. SDS-PAGE of the recombinant strain *E. coli* C01-C07.**

336 Lane M represents protein marker, lanes 1-7 correspond to the cell lysate supernatants of *E. coli*
337 C01–C07, respectively. α: *Ec*ADH^{M7} (36.3 kDa); β: *Ec*PaTA^{W4} (49.7 kDa); γ: *Sc*GluDH (49.6 kDa);
338 α*: *Ec*ADH$^{M7}{}_{HisTag}$ (38.2 kDa); β*: *Ec*PaTA$^{W4}{}_{HisTag}$ (51.5 kDa). The asterisk (*) indicates enzymes
339 carrying an N-terminal 6×His tag.

340

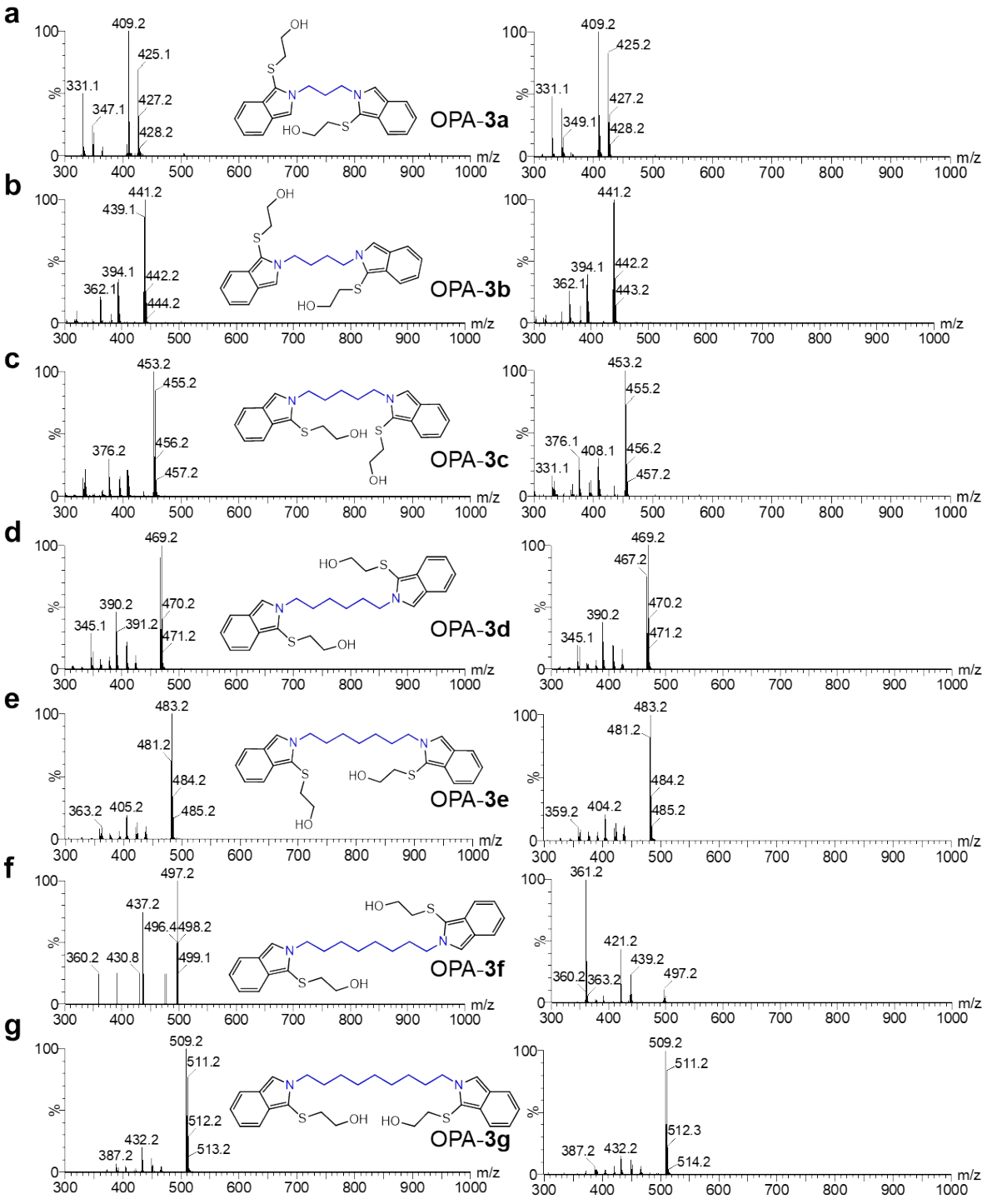

Figure S10. LC-MS spectra of OPA-3a to OPA-3g.

The spectrum on the left represents the standard sample, while the one on the right represents the reaction sample. (a) OPA-**3a**, $[M+H]^+$=427.14. (b) OPA-**3b**, $[M+H]^+$=441.16. (c) OPA-**3c**, $[M+H]^+$=455.17. (d) OPA-**3d**, $[M+H]^+$=469.19. (e) OPA-**3e**, $[M+H]^+$=483.21. (f) OPA-**3f**, $[M+H]^+$=497.22. (g) OPA-**3g**, $[M+H]^+$=511.24.

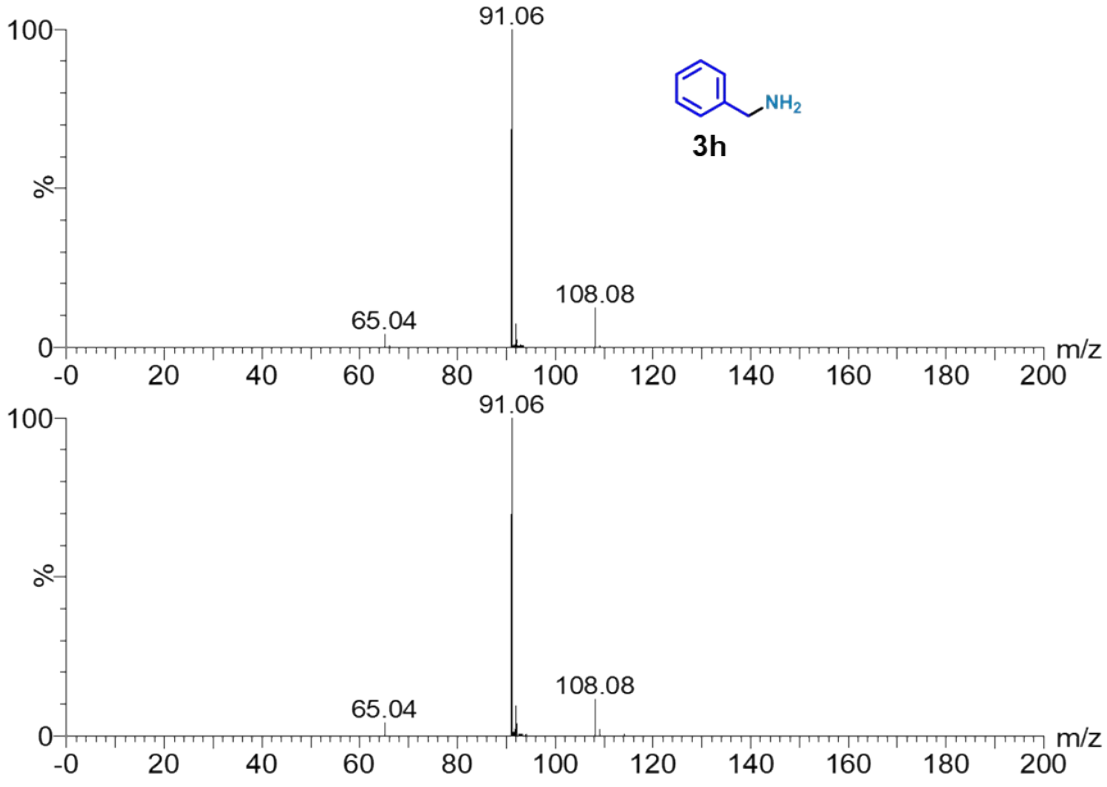

Figure S11. LC-MS spectra of 3h.

The spectrum above represents the standard sample, while the one below represents the reaction sample. $[M+H]^+$=108.07.

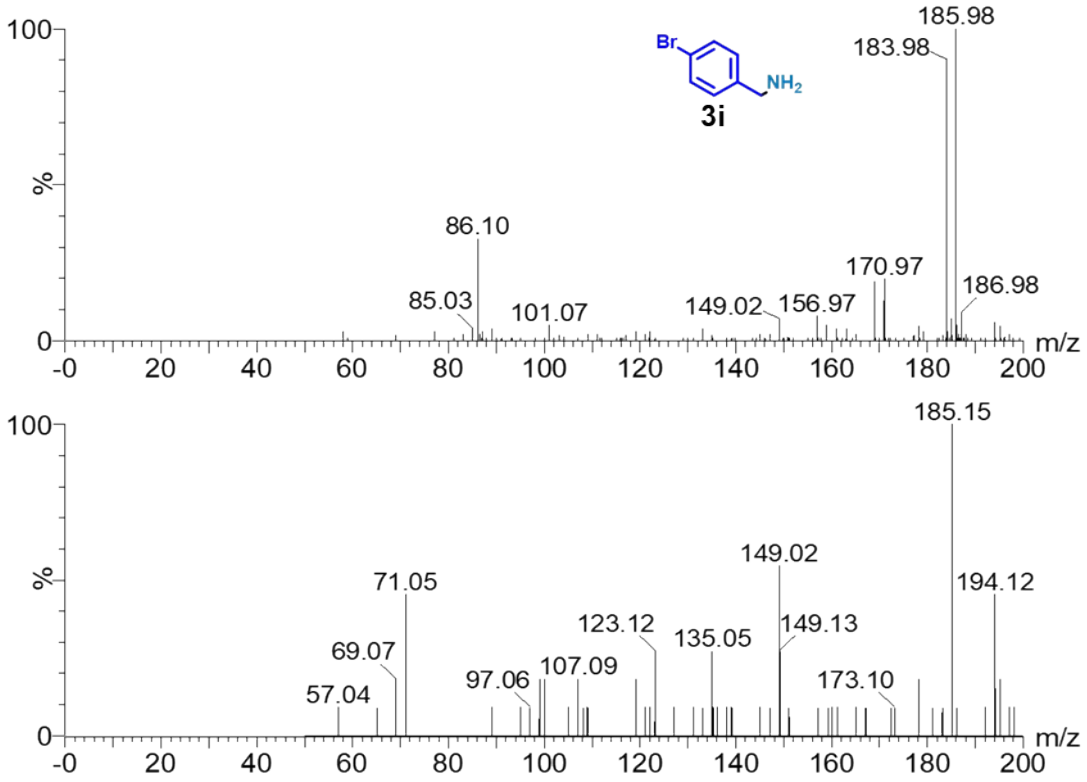

352

353 **Figure S12. LC-MS spectra of 3i.**

354 The spectrum above represents the standard sample, while the one below represents the

355 reaction sample. $[M+H]^+$=185.98.

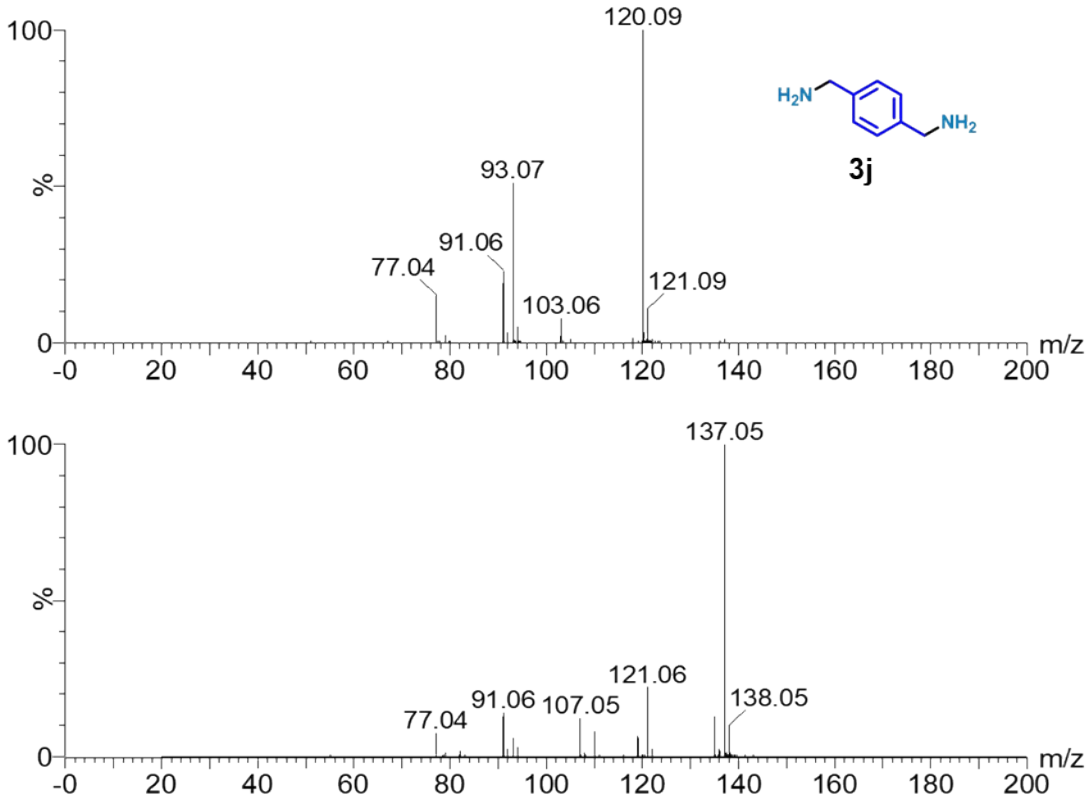

356

357 **Figure S13. LC-MS spectra of 3j.**

358 The spectrum above represents the standard sample, while the one below represents the

359 reaction sample. $[M+H]^+$=137.10.

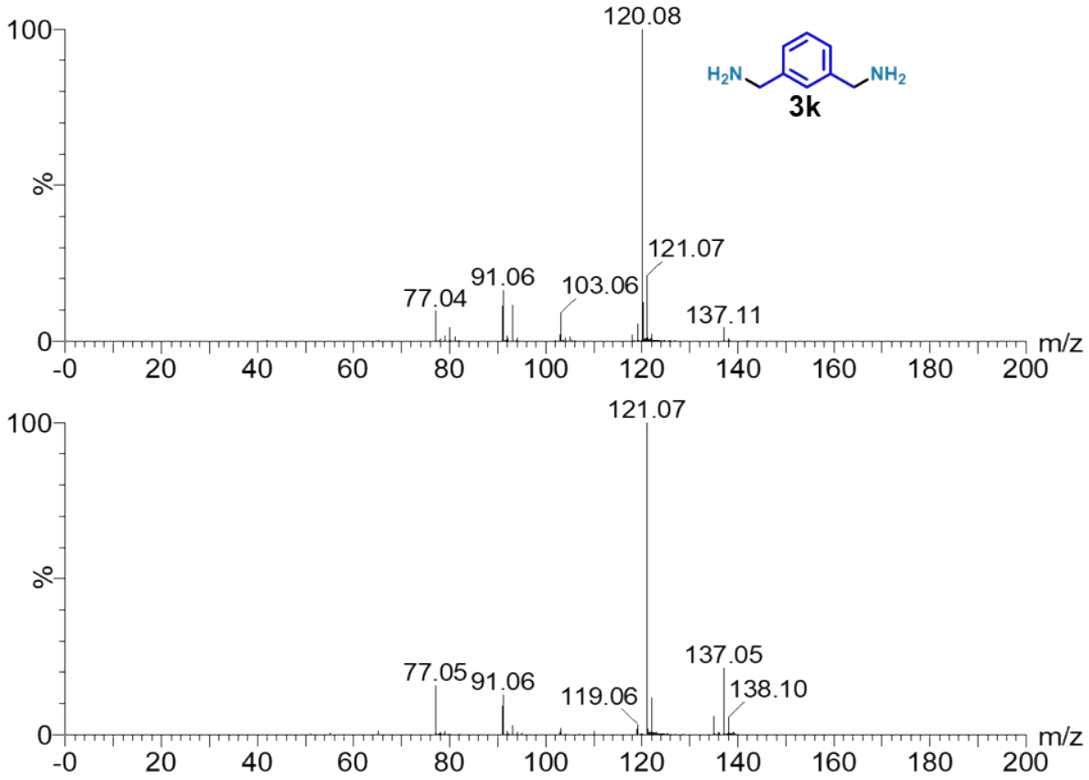

Figure S14. LC-MS spectra of 3k.

The spectrum above represents the standard sample, while the one below represents the reaction sample. $[M+H]^+$=137.10.

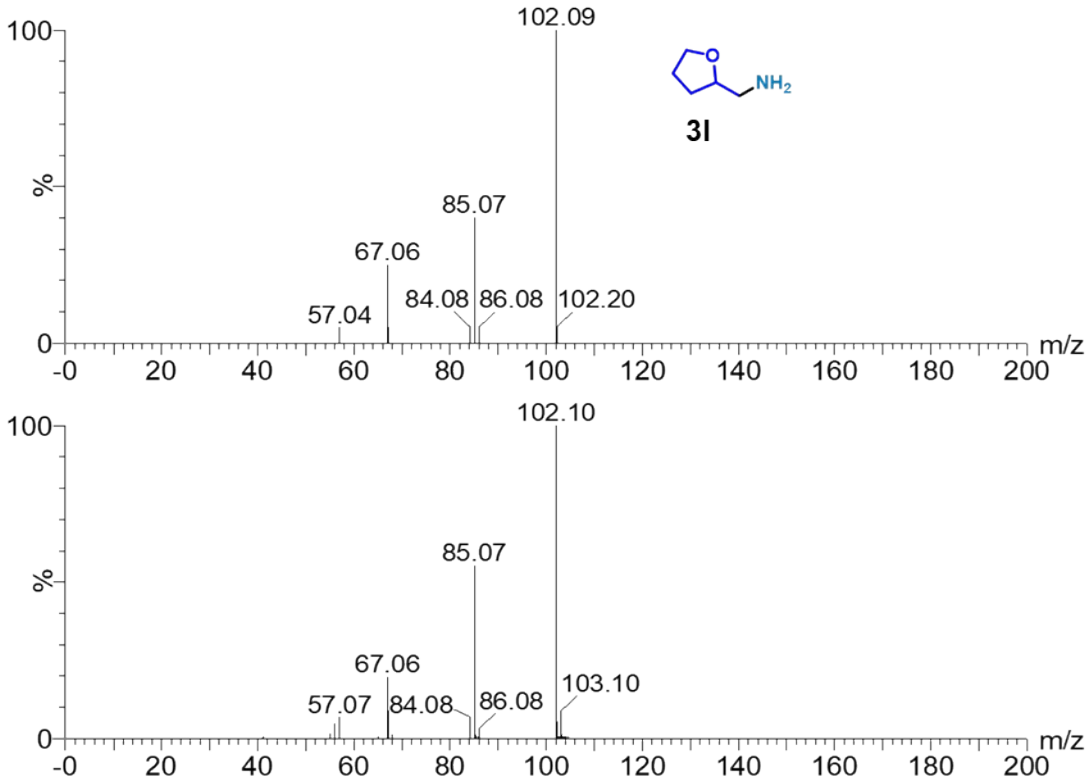

Figure S15. LC-MS spectra of 3l.

The spectrum above represents the standard sample, while the one below represents the reaction sample. $[M+H]^+$=102.08.

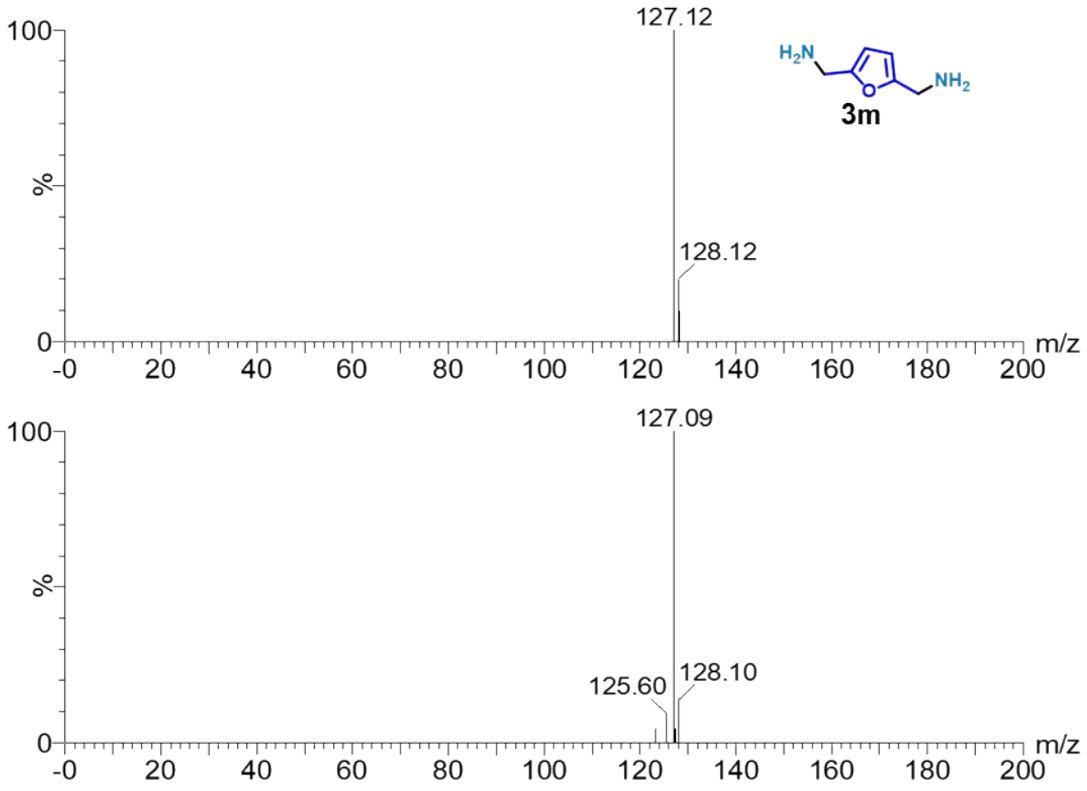

Figure S16. LC-MS spectra of 3m.

The spectrum above represents the standard sample, while the one below represents the reaction sample. $[M+H]^+$=127.08.

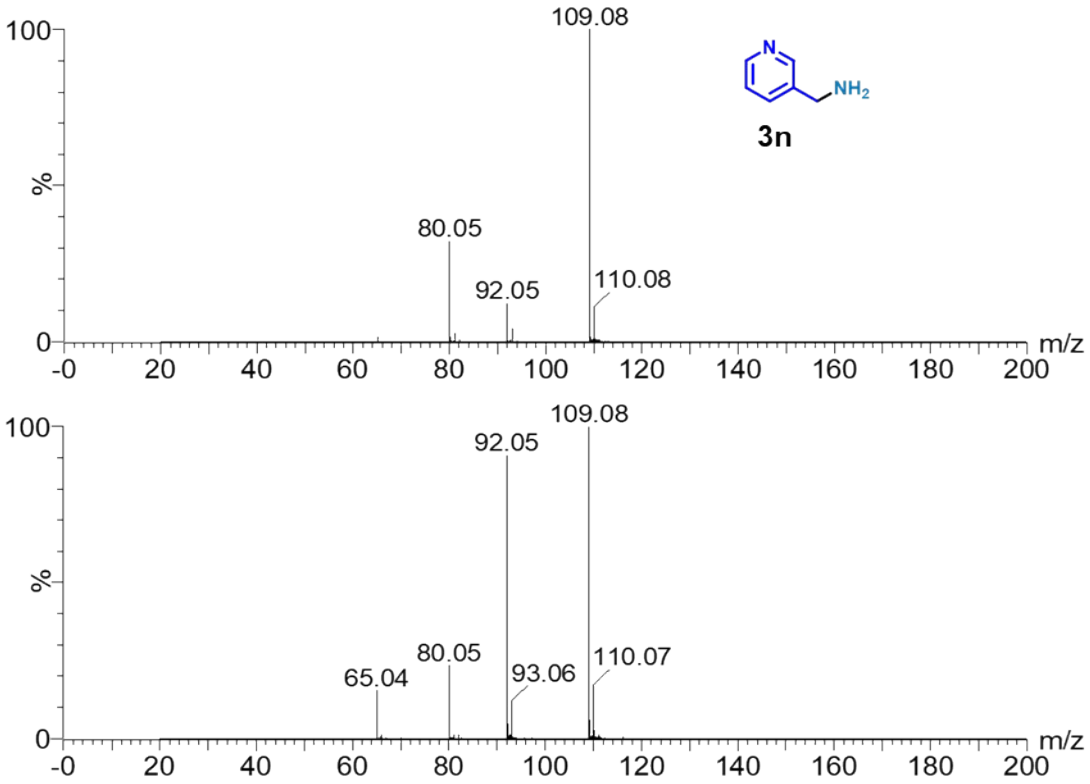

374

375 **Figure S17. LC-MS spectra of 3n.**

376 The spectrum above represents the standard sample, while the one below represents the

377 reaction sample. $[M+H]^+$=109.08.

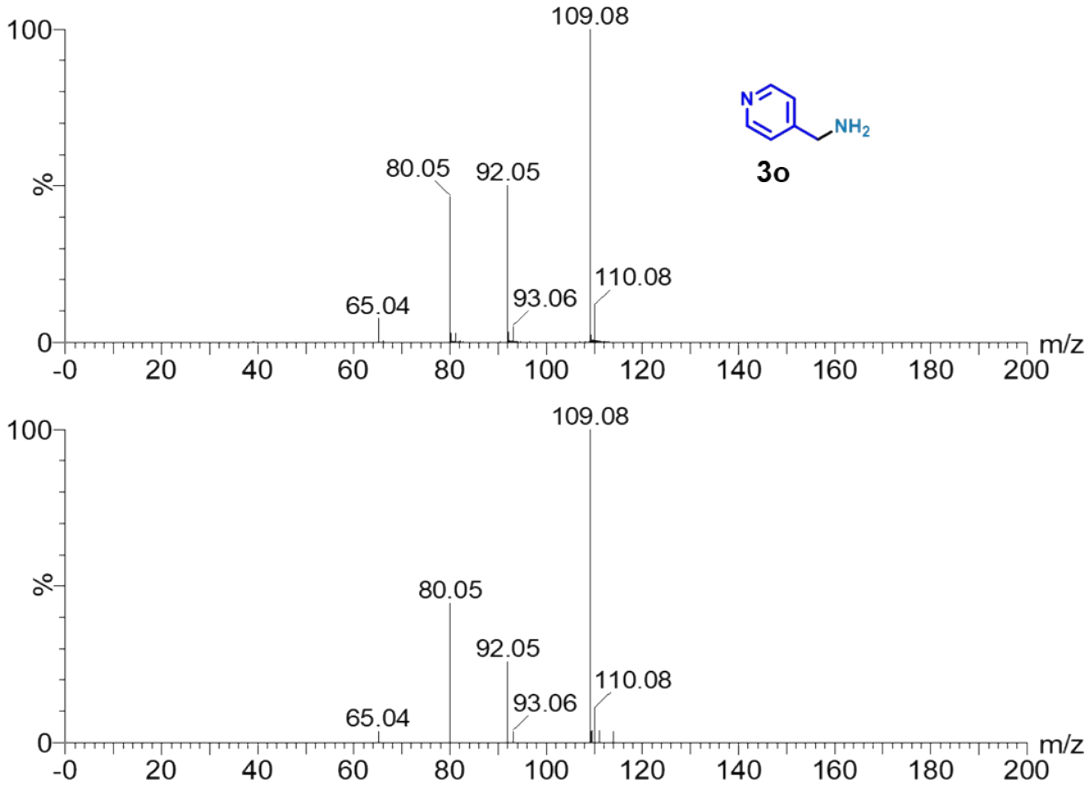

Figure S18. LC-MS spectra of 3o.

The spectrum above represents the standard sample, while the one below represents the reaction sample. $[M+H]^+$=109.07.

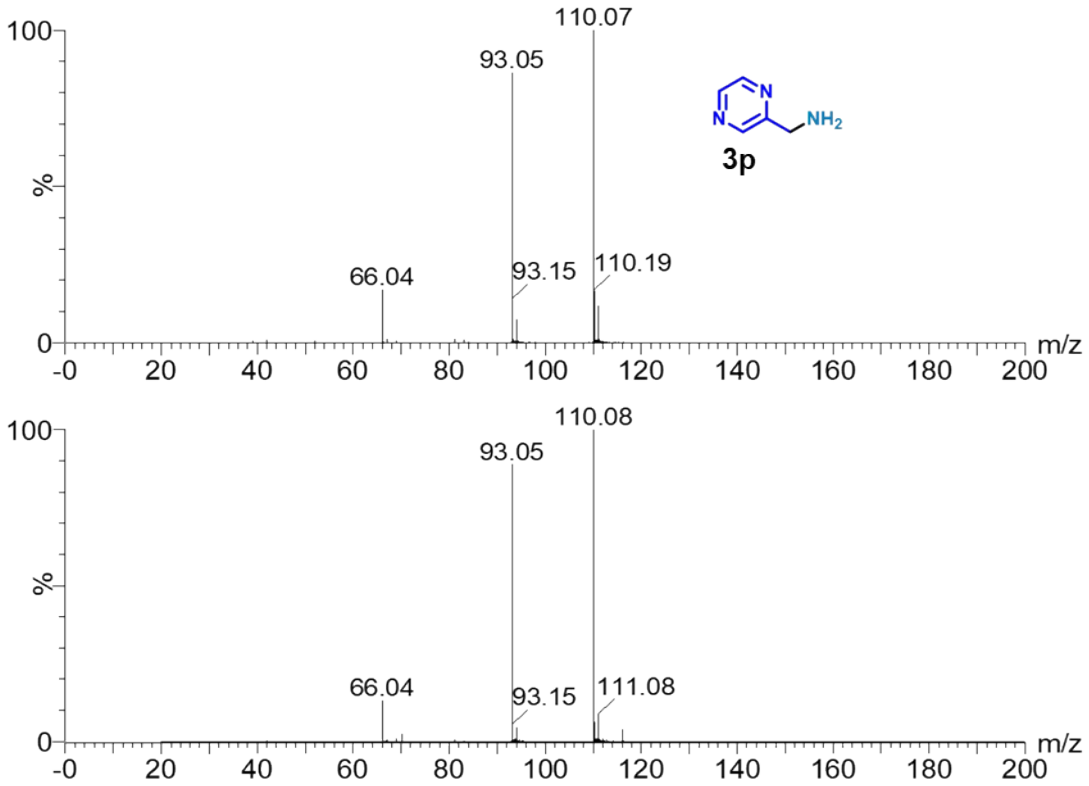

382

383 **Figure S19. LC-MS spectra of 3p.**

384 The spectrum above represents the standard sample, while the one below represents the

385 reaction sample. $[M+H]^+$=110.06.

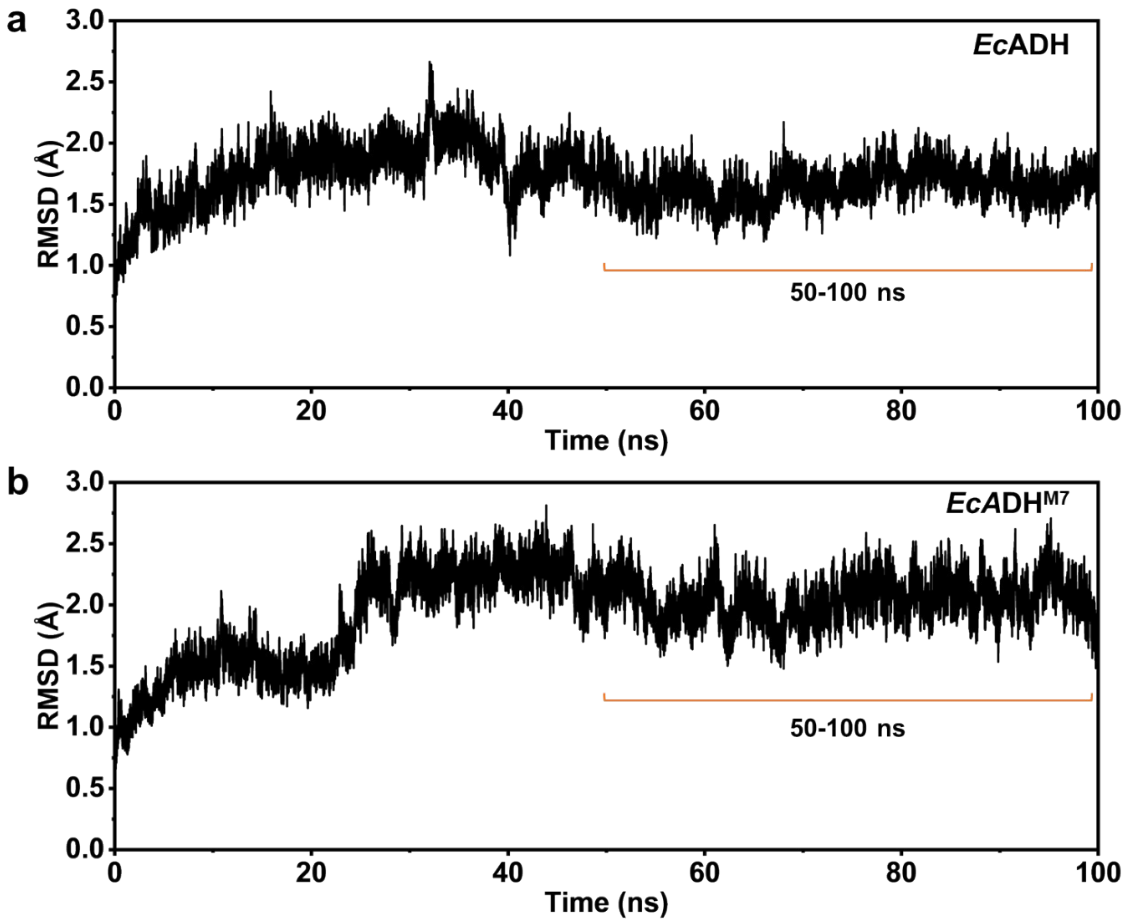

386

387 **Figure S20. Root-mean-square deviation (RMSD) of backbone heavy atoms relative to the**

388 **first snapshot during 100 ns MD simulation of *Ec*ADH and *Ec*ADH^{M7}.**

389 (a) *Ec*ADH-NADP$^+$-**2a** ternary complex and (b) *Ec*ADH^{M7}-NADP$^+$-**2a** ternary complex. During the

390 50-100 ns period, the system remains in a stable phase.

391

Reference

1. Jorgensen, W.L., Chandrasekhar, J., Madura, J.D., Impey, R.W., and Klein, M.L.. Comparison of simple potential functions for simulating liquid water. *J. Chem. Phys.* **1983,** 79, 926-935.
2. Frisch, M.J., Trucks, G.W., Schlegel, H.B., Scuseria, G.E., Robb, M.A., Cheeseman, J.R., Scalmani, G., Barone, V., Petersson, G.A., Nakatsuji, H., et al. *Gaussian 16 Rev. C.01.* **2016**
3. Morris, G.M., Goodsell, D.S., Halliday, R.S., Huey, R., Hart, W.E., Belew, R.K. and Olson, A.J., Automated docking using a Lamarckian genetic algorithm and an empirical binding free energy function. *J. Comput. Chem.* **1998**, 19: 1639-1662.
4. Morris, G. M., Huey, R., Lindstrom, W., Sanner, M. F., Belew, R. K., Goodsell, D. S., & Olson, A. J.. AutoDock4 and AutoDockTools4: Automated docking with selective receptor flexibility. J. *Comput. Chem.* **2009**, 30(16), 2785–2791.
5. Case, D., Ben-Shalom, I., Brozell, S.R., Cerutti, D.S., Cheatham, T., Cruzeiro, V.W.D., Darden, T., Duke, R., Ghoreishi, D., Gilson, M., et al. *Amber 2018.* **2018**
6. Jakalian, A., Jack, D. B., & Bayly, C. I., Fast, efficient generation of high-quality atomic charges. AM1-BCC model: II. Parameterization and validation. *J. Comput. Chem.* **2002**, 23(16), 1623–1641.
7. Wang, J., Wolf, R. M., Caldwell, J. W., Kollman, P. A., & Case, D. A., Development and testing of a general amber force field. *J. Comput. Chem.* **2004**, 25(9), 1157–1174.
8. Darden, T., York, D., and Pedersen, L., Particle mesh Ewald: An N·log(N) method for Ewald sums in large systems. *J. Chem. Phys.* **1993**, 98, 10089-10092.
9. Chae, T. U.; Kim, W. J.; Choi, S.; Park, S. J.; Lee, S. Y., Metabolic engineering of *Escherichia coli* for the production of 1,3-diaminopropane, a three carbon diamine. *Sci. Rep.* **2015,** *5* (1), 13040.
10. Noh, M.; Yoo, S. M.; Kim, W. J.; Lee, S. Y., Gene expression knockdown by modulating synthetic small rna expression in *Escherichia coli*. *Cell Syst.* **2017,** *5* (4), 418-426.e4.

11. Kim, H. T.; Baritugo, K.-A.; Oh, Y. H.; Hyun, S. M.; Khang, T. U.; Kang, K. H.; Jung, S. H.; Song, B. K.; Park, K.; Kim, I.-K.; Lee, M. O.; Kam, Y.; Hwang, Y. T.; Park, S. J.; Joo, J. C., Metabolic engineering of *Corynebacterium glutamicum* for the high-Level production of cadaverine that can be used for the synthesis of biopolyamide 510. *ACS Sustainable Chem. Eng.* **2018,** *6* (4), 5296-5305.
12. Xiao, K.; Wang, D.; Liu, X.; Kang, Y.; Luo, R.; Hu, L.; Peng, Z., Novel bioproduction of 1,6-hexamethylenediamine from L-lysine based on an artificial one-carbon elongation cycle. *ACS Omega* **2024,** *9* (39), 40970-40979.
13. Sarak, S.; Pagar, A. D.; Khobragade, T. P.; Jeon, H.; Giri, P.; Lim, S.; Patil, M. D.; Kim, Y.; Kim, B. G.; Yun, H., A multienzyme biocatalytic cascade as a route towards the synthesis of α,ω-diamines from corresponding cycloalkanols. *Green Chem.* **2023,** *25* (2), 543-549.
14. Zhang, Z. W.; Fang, L.; Wang, F.; Deng, Y.; Jiang, Z. B.; Li, A. T., Transforming inert cycloalkanes into α,ω-diamines by designed enzymatic cascade catalysis. *Angew. Chem. Int. Ed.* **2023,** *62* (16), 10.
15. Kim, Y. C.; Yoo, H.-W.; Park, B. G.; Sarak, S.; Hahn, J.-S.; Kim, B.-G.; Yun, H., One-Pot Biocatalytic Route from Alkanes to α,ω-Diamines by Whole-Cell Consortia of Engineered Yarrowia lipolytica and *Escherichia coli*. *ACS Synth. Biol* **2024,** *13* (7), 2188-2198.
16. Hwang, S.-Y.; Woo, J.-M.; Choi, G. E.; Oh, D.-K.; Seo, J.-H.; Park, J.-B., Biological Reaction Engineering for the Preparation of C9 Chemicals from Oleic Acid: 9-Aminononanoic Acid, 1,9-Nonanediol, 9-Amino-1-nonanol, and 1,9-Diaminononane. *ACS Catal.* **2024,** *14* (6), 4130-4138.
17. Gopal, M. R.; Dickey, R. M.; Butler, N. D.; Talley, M. R.; Nakamura, D. T.; Mohapatra, A.; Watson, M. P.; Chen, W.; Kunjapur, A. M., Reductive enzyme cascades for valorization of polyethylene terephthalate deconstruction products. *ACS Catal.* **2023,** *13* (7), 4778-4789.
18. Giri, P.; Lim, S.; Khobragade, T. P.; Pagar, A. D.; Patil, M. D.; Sarak, S.; Jeon, H.; Joo, S.; Goh, Y.; Jung, S.; Jang, Y. J.; Choi, S. B.; Kim, Y. C.; Kang, T. J.; Heo,

Y. S.; Yun, H., Biocatalysis enables the scalable conversion of biobased furans into various furfurylamines. *Nat. Commun.* **2024,** *15* (1), 6371.

19. Yang, W.; Liu, H.; Li, S.; Luo, J.; Liang, C., Selective Hydrogenation of Adiponitrile to Hexamethylenediamine by Supported Co Catalyst under Alkali-Free Conditions. *Industrial & Engineering Chemistry Research* **2024,** *63* (26), 11374-11383.
20. Wu, R.; Wang, H.; Li, H.; Tian, X. Catalyst containing skeleton Ni for preparation of 1,4-diaminomethyl benzene and preparation method thereof. CN102179259, **2011**.
21. Robert, X., & Gouet, P. Deciphering key features in protein structures with the new ENDscript server. *NucleicAcids Res.* **2014,** 42, W320–W324.